*2021 International Nuclear Atlantic Conference – INAC 2021*
*Virtual meeting, Brazil, November 29 – December 2, 2021*

# XRF data simulation to calculate pigment layer thickness in works of art.

Ana Letícia C. de Oliveira[1], Renato P. de Freitas[2],André R. Pimenta[3] and Marcelino J. dos Anjos[4]

[1]*annalecastro@hotmail.com*
*Rio de Janeiro State University (UERJ)*
*R. São Francisco Xavier, 524 - Maracanã, Rio de Janeiro - RJ, 20550-013*

[2]*renato.freitas@ifrj.edu.br*
*Federal Institute of Education and Science of Rio de Janeiro (IFRJ / LISCOMP - RJ)*
*R. Sebastião de Lacerda, S/N - Fábrica, Paracambi - RJ, 26600-000*

[3]*andre.pimenta@ifrj.edu.br*
*Federal Institute of Education and Science of Rio de Janeiro (IFRJ / LISCOMP - RJ)*
*R. Sebastião de Lacerda, S/N - Fábrica, Paracambi - RJ, 26600-000*

[4]*marclin@uerj.com.br*
*Rio de Janeiro State University (UERJ)*
*R. São Francisco Xavier, 524 - Maracanã, Rio de Janeiro - RJ, 20550-013*

## 1. Introduction

The investigation of works of art and objects of archaeological value makes it possible to obtain information about the composition of these artifacts, the techniques used in the manufacturing process, in addition to helping to identify counterfeiting and restoration regions [1,2]. In artifacts such as canvases, sculptures, paintings, it is common for them to be manufactured using multilayers of pigments, such as the use of a canvas preparation layer, used to receive a visible polychromy of the canvas. Therefore, the characterization of the multilayers present in a work of art brings valuable information about the creative process, in addition to being useful in the verification of pigment layers used in the work's restoration process.

Due to the historical value of these objects, the scientific analysis of these works must take place through non-destructive testing techniques. One of the most used analysis techniques in archaeometry is X-Ray Fluorescence (XRF). This technique is still being used, due to technological advances that have occurred, making it easier to use in works of art [3–6]. It is possible to deepen the information provided by the XRF data, from theoretical approaches [7–9]. For example, the calculation of the ratios of the areas of the energy peaks Kα, Kβ or Lα, Lβ of a determined chemical element allows us to conclude information about the thickness of the analyzed pigment layer [8,10–13].

The study of pigment thickness calculation has been widely used in works of art, especially in the calculation of thicknesses of gold over lead white pigment [13–17]. For this, the ratio of the areas of the Lα and Lβ peaks of lead identified by the XRF analysis is used. Determining the thickness of the layer makes it possible to investigate the process of creation of pigment layers, thus facilitating the process of conservation and restoration of the work. In addition, this approach contributes to the development of methods, which employ non-destructive techniques, such as XRF, to calculate layer thickness.

## 2. Methodology

### 2.1. Calculation of layer thicknesses from attenuation data of a second pigment layer.

In this work, the case of attenuation by the second layer will be addressed. This case is called this because it is the approach of attenuation of the X-ray beam for two layers: a base layer and a second layer,

called coating. In this case, the X-ray beam emitted will result from the attenuation suffered by the base layer and finally by the coating layer.

To demonstrate the development of the attenuation equation by the second layer, the self-attenuation equation will be used [11,18], added by the term referring to the coating layer. To better exemplify the case, a case will be considered with the base layer composed of the white lead pigment and the coating layer being a chromium oxide layer.

$$Pb\left(\frac{K_\alpha}{K_\beta}\right) = \underbrace{Pb\left(\frac{K_{0\alpha}}{K_{0\beta}}\right).\left[\frac{\mu_0 + \mu_2}{\mu_0 + \mu_1}\right].\left[\frac{1- e^{-\rho x(\mu_0+\mu_1)}}{1- e^{-\rho x(\mu_0+\mu_2)}}\right]}_{Part\ 1}.\frac{\left[\left(e^{-\mu_{au}(E_0)\frac{\rho_{cr}.d_{cr}}{\sin\varphi}}\right).\left(e^{-\mu_3\frac{\rho_{cr}.d_{cr}}{\sin\varphi}}\right)\right]}{\left[\left(e^{-\mu_{au}(E_0)\frac{\rho_{cr}.d_{cr}}{\sin\varphi}}\right).\left(e^{-\mu_4\frac{\rho_{cr}.d_{cr}}{\sin\varphi}}\right)\right]} \quad (1)$$

$$Pb\left(\frac{L_\alpha}{L_\beta}\right) = \underbrace{Pb\left(\frac{L_{0\alpha}}{L_{0\beta}}\right).\left[\frac{\mu_0 + \mu_2}{\mu_0 + \mu_1}\right].\left[\frac{1- e^{-\rho x(\mu_0+\mu_1)}}{1- e^{-\rho x(\mu_0+\mu_2)}}\right]}_{Part\ 1}.\frac{\left[\left(e^{-\mu_{au}(E_0)\frac{\rho_{cr}.d_{cr}}{\sin\varphi}}\right).\left(e^{-\mu_3\frac{\rho_{cr}.d_{cr}}{\sin\varphi}}\right)\right]}{\left[\left(e^{-\mu_{au}(E_0)\frac{\rho_{cr}.d_{cr}}{\sin\varphi}}\right).\left(e^{-\mu_4\frac{\rho_{cr}.d_{cr}}{\sin\varphi}}\right)\right]} \quad (2)$$

$\boldsymbol{\mu_{au}}(E_0)$ is the attenuation coefficient of the gold layer for the E0 energy of the X-ray tube;; $\boldsymbol{\mu_3}$ is the attenuation coefficient of the chromium oxide layer for the Kα or Lα energy of the base layer element; $\boldsymbol{\mu_4}$ is the attenuation coefficient of the chromium oxide layer for the Kβ or Lβ energy of the base layer element; $\mathbf{d_{cr}}$ is the thickness of the chromium oxide layer; **φ** is the angle of incidence of the X-ray beam; **φ** is the exit angle of the X-ray beam; **x** base layer thickness.

In this work, the thickness x of the base layer will be considered as coarse thickness. Thus, part 1 of equations (1) and (2) can be replaced by reason $Pb(K\alpha/K\beta)_\infty$ e $Pb(L\alpha/L\beta)_\infty$.

$$Pb\left(\frac{K_\alpha}{K_\beta}\right) = Pb\left(\frac{K_\alpha}{K_\beta}\right)_\infty.\left[e^{\frac{-(\mu_3-\mu_4)\rho_{cr}.d_{cr}}{\sin\varphi}}\right] \quad (3)$$

$$Pb\left(\frac{L_\alpha}{L_\beta}\right) = Pb\left(\frac{L_\alpha}{L_\beta}\right)_\infty.\left[e^{\frac{-(\mu_3-\mu_4)\rho_{cr}.d_{cr}}{\sin\varphi}}\right] \quad (4)$$

## 3. Results and Discussion

### 3.1 Second Layer Attenuation Results

For attenuation by the second layer, layers of chromium oxide were painted over a thick layer of lead white on a canvas. For each layer, XRF spectra were collected. As the chromium oxide layers were painted over lead white, to identify the chromium oxide thickness it is necessary to calculate the Pb(Lα/Lβ) ratio. This experimental ratio was calculated using the ratio between the Lα and Lβ peak area values of Pb. These values will be identified as the experimental Pb(Lα/Lβ) ratio.

The XMI-MSIM [17] program was used to simulate XRF spectra. Spectra were simulated considering the lead white $(PbCO_3)_2{\cdot}Pb(OH)_2$ layer 300 µm thick, and the chromium oxide thickness ranged from 10 to 80 µm. For each simulated spectrum, the areas of the Lα and Lβ peaks of Pb were calculated and then the Pb(Lα/Lβ) ratio was performed for each XRF spectrum. With this, it is possible to assemble the graph of figure 3, which relates the simulated Pb(Lα/Lβ) ratio with the chromium oxide ($Cr_2O_3$) thickness values.

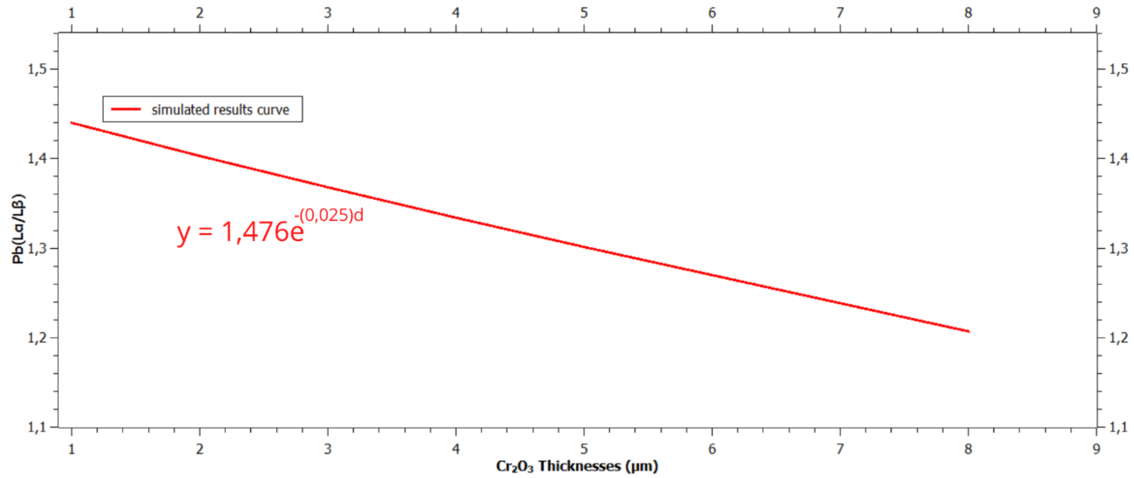


*Figure 1: graph of simulated Pb(Lα/Lβ) values versus chromium oxide thickness.*

The graph in figure 1 is described by the curve equation as y= $1.476e^{(-0.025)d}$ . Using the classical equation (4), it is possible to observe the similarity between the mathematical model of the two equations. For a better comparison between the two equations, the theoretical values referring to the chromium oxide layer in equation (4) will be used. Below are the two equations for comparing the theoretical equation and the simulated curve equation.

*Theoretical equation of attenuation by the second layer*

$$Pb\left(\frac{L_\alpha}{L_\beta}\right) = 1,461\,.\,e^{(-0,030)d_{cr}} \quad (10)$$

*Equation obtained by the simulated curve*

$$Pb\left(\frac{L_\alpha}{L_\beta}\right) = 1,476\,.\,e^{-(0,025)d_{cr}} \quad (11)$$

It is possible to identify the similarity between the values identified in the two equations. It can be concluded that the simulated curve presents a behavior consistent with the theoretical equation. This makes the simulated results possible for comparison with experimental results, since the behavior of the simulated curve respects the behavior of the theoretical equation. From this observation, the simulated curve equation was used as the standard equation to identify the thicknesses of the experimental chromium oxide layers, as shown in Figure 2.

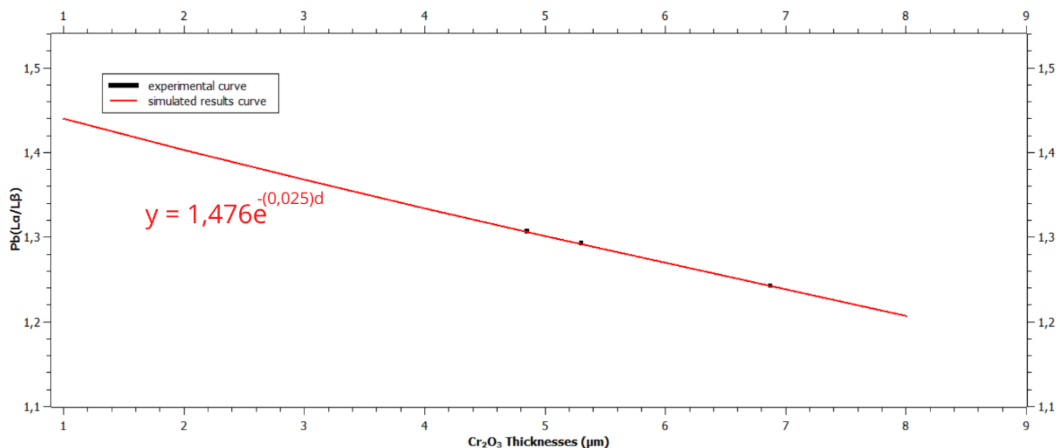


*Figure 2: graph of simulated Pb(Lα/Lβ) values versus chromium oxide thickness.*

The results of the experimental Pb(Lα/Lβ) ratio, identified in the simulated curve equation, were the values associated with samples with 1 layer, 2 layers and 3 layers of chromium oxide. Being related the thicknesses of 4.85 ± 0.01 μm for the experimental Pb(Lα/Lβ) ratio of 1 layer, 5.30 ± 0.01 μm for the experimental Pb(Lα/Lβ) ratio of 2 layers and 6 .87 ± 0.01 μm for the 3-layer experimental Pb(Lα/Lβ) ratio. From the third chromium oxide layer onwards, the values presented for the experimental Pb(Lα/Lβ) ratio no longer respect the behavior of the curve, becoming values with no common behavior between them. The justification for this behavior was the increase in the thickness of the chromium oxide layer, making a sample thick.

## 4. Conclusions

Through this study, it was possible to verify the feasibility of employing the method of differential attenuation of X-rays characteristic of an element, to determine the thickness of pigment layers used in screens. Through theoretical modeling, it was possible to verify the application of equation (1) and equation (2) to determine pigment layer thickness, associated with comparison with simulated results.

A comparison approach between experimental results and simulated results was used. This approach was very satisfactory for the case studied. Comparing with the results of the experimental Pb(Lα/Lβ) ratio, it was possible to determine the thickness of 3 layers of chromium oxides. The study also allowed to verify the effectiveness of computer simulation of XRF, using the XMI-MSIM software. It is important to emphasize that simulation was an essential tool in the development of this work. If computer simulation were not used, it would not be possible to compare experimental and theoretical results.

## Acknowledgements

The authors thank CAPES for the financial support for the development of the work, whose subject was the subject of the master's thesis, developed at the State University of Rio de Janeiro (UERJ).

## References

[1] R. Klockenkämper, A. Von Bohlen, L. Moens, Analysis of Pigments and Inks on Oil Paintings and Historical Manuscripts Using Total Reflection X-ray Fluorescence Spectrometry, X-Ray Spectrom. 29 (2000) 119–129. https://doi.org/10.1002/(SICI)1097-4539(200001/02)29:1<119::AID-XRS400>3.0.CO;2-W.

[2] C.F. Calza, Desenvolvimento de sistemas portátil de fluorescência de raios X com aplicações em arqueometria, (2007) 163.

[3] M.J. Anjos, Micro-XRF analysis of a Brazilian polychrome sculpture, n.d.

[4] R.P. Freitas, I.M. Ribeiro, C. Calza, A.L. Oliveira, V.S. Felix, D.S. Ferreira, A.R. Pimenta, R. V. Pereira, M.O. Pereira, R.T. Lopes, Analysis of a Brazilian baroque sculpture using Raman spectroscopy and FT-IR, Spectrochim. Acta - Part A Mol. Biomol. Spectrosc. 154 (2016) 67–71. https://doi.org/10.1016/j.saa.2015.10.013.

[5] R.P. Freitas, V.S. Felix, M.O. Pereira, R.S. Santos, A.L. Oliveira, E.A.S. Gonçalves, D.S. Ferreira, A.R. Pimenta, L.O. Pereira, M.J. Anjos, Micro-XRF analysis of a Brazilian polychrome sculpture, Microchem. J. 149 (2019) 104020. https://doi.org/10.1016/j.microc.2019.104020.

[6] R. Molari, C.R. Appoloni, S.H. Rodriguez, Non-destructive portable X-ray fluorescence analysis of the Portrait of a Young Man with a Golden Chain (c. 1635) by Rembrandt and/or atelier, Appl. Radiat. Isot. 165 (2020) 109346. https://doi.org/10.1016/j.apradiso.2020.109346.

[7] M.O. Pereira, V.S. Felix, A.L. Oliveira, D.S. Ferreira, A.R. Pimenta, C.S. Carvalho, F.L. Silva, C.A. Perez, D. Galante, R.P. Freitas, Investigating counterfeiting of an artwork by XRF, SEM-EDS, FTIR and synchrotron radiation induced MA-XRF at LNLS-BRAZIL, Spectrochim. Acta - Part A Mol. Biomol. Spectrosc. 246 (2021). https://doi.org/10.1016/j.saa.2020.118925.

[8] S. Pessanha, T.I. Madeira, M. Manso, M. Guerra, A. Le Gac, M.L. Carvalho, Comparison of gold leaf thickness in Namban folding screens using X-ray fluorescence, Appl. Phys. A Mater. Sci. Process. 116 (2014) 1053–1058. https://doi.org/10.1007/s00339-014-8531-z.

[9] S.H. Rodriguez, C.R. Appoloni, P.H.O.V. Campos, B. Gonçalves, E.A.M. Kajiya, R. Molari, M.A.

Rizzutto, C. Winter, Non-Destructive and portable analyses helping the study and conservation of a Saraceni copper plate painting in the São Paulo museum of art, Microchem. J. 155 (2020) 104787. https://doi.org/10.1016/j.microc.2020.104787.
[10] R. Cesareo, C. Calza, M. Dos Anjos, R.T. Lopes, A. Bustamante, J. Fabian S., W. Alva, L. Chero Z., Pre-Columbian alloys from the royal tombs of Sipán; energy dispersive X-ray fluorescence analysis with a portable equipment, Appl. Radiat. Isot. (2010). https://doi.org/10.1016/j.apradiso.2009.09.005.
[11] R. Cesareo, J.T. De Assis, C. Roldán, A.D. Bustamante, A. Brunetti, N. Schiavon, Multilayered samples reconstructed by measuring Kα/K β or Lα/Lβ X-ray intensity ratios by EDXRF, 2013. https://doi.org/10.1016/j.nimb.2013.06.019.
[12] F. Lopes, F.L. Melquiades, C.R. Appoloni, R. Cesareo, M. Rizzutto, T.F. Silva, Thickness determination of gold layer on pre-Columbian objects and a gilding frame, combining pXRF and PLS regression, X-Ray Spectrom. 45 (2016) 344–351. https://doi.org/10.1002/xrs.2711.
[13] S. Pessanha, M. Guerra, S. Longelin, A. Le Gac, M. Manso, M.L. Carvalho, Determination of gold leaf thickness in a Renaissance illumination using a nondestructive approach, X-Ray Spectrom. 43 (2013) 79–82. https://doi.org/10.1002/xrs.2518.
[14] S.A.B. Lins, G.E. Gigante, R. Cesareo, S. Ridolfi, A. Brunetti, Testing the accuracy of the calculation of gold leaf thickness by mc simulations and MA-XRF scanning, Appl. Sci. 10 (2020). https://doi.org/10.3390/app10103582.
[15] S.A. Barcellos Lins, S. Ridolfi, G.E. Gigante, R. Cesareo, M. Albini, C. Riccucci, G. di Carlo, A. Fabbri, P. Branchini, L. Tortora, Differential X-Ray Attenuation in MA-XRF Analysis for a Non-invasive Determination of Gilding Thickness, Front. Chem. 8 (2020) 1–9. https://doi.org/10.3389/fchem.2020.00175.
[16] F.A.C.R. d. A. Sanches, R.C. Nardes, H.S.G. Filho, R.S. dos Santos, O.M.O. de Araújo, A.S. Machado, T. Calgam, R. Bueno, C. Canellas, E.A.S. Gonçalves, J.T. Assis, R.P. de Freitas, D.F. de Oliveira, R.T. Lopes, M.J. dos Anjos, Characterization of a sacred statuette replica of "Nossa Senhora da Conceição Aparecida" using X-ray spectrometry techniques, Radiat. Phys. Chem. 167 (2020) 1–6. https://doi.org/10.1016/j.radphyschem.2019.04.016.
[17] S. Pessanha, I. Queralt, M.L. Carvalho, J.M. Sampaio, Determination of gold leaf thickness using X-ray fluorescence spectrometry: Accuracy comparison using analytical methodology and Monte Carlo simulations, Appl. Radiat. Isot. 152 (2019) 6–10. https://doi.org/10.1016/j.apradiso.2019.06.014.
[18] R. Cesareo, M.A. Rizzutto, A. Brunetti, D. V. Rao, Metal location and thickness in a multilayered sheet by measuring Kα/Kβ, Lα/Lβ and Lα/Lγ X-ray ratios, Nucl. Instruments Methods Phys. Res. Sect. B Beam Interact. with Mater. Atoms. 267 (2009) 2890–2896. https://doi.org/10.1016/j.nimb.2009.06.119.